

Variational evidence for spin liquids in frustrated lattices

D. M. Deaven

Department of Physics, Ames Laboratory United States Department of Energy, Ames, Iowa 50011

D. S. Rokhsar

Department of Physics, University of California, Berkeley, California 94720

(Received 22 December 1995)

We present a Gutzwiller-projected variational state appropriate for Heisenberg quantum antiferromagnets which incorporates staggered magnetization as a continuous variational parameter. Although we obtain Néel-ordered ground states with appropriate sublattice magnetization on the square, honeycomb, and triangular lattice spin- $\frac{1}{2}$ quantum antiferromagnets, we find no such order on the *kagomé* lattice, providing evidence that the ground state on the *kagomé* lattice is disordered. The spin-spin correlations we obtain for spins separated by more than a lattice constant are similar to those obtained by exact diagonalization of small clusters. [S0163-1829(96)07821-6]

A fundamental issue in quantum antiferromagnetism is the existence of long-range order in the ground state. In one dimension, the ground state of the linear chain spin $\frac{1}{2}$ quantum antiferromagnet (QAFM) is disordered with unbroken translational symmetry^{1,2} – a “spin-liquid.” To date no two-dimensional lattice QAFM has been shown to have a spin-liquid ground state, though it is generally believed that lattices with low coordination number and frustrated classical antiferromagnetism are the best candidates. The search for a two-dimensional spin liquid has been refueled by exotic theories of cuprate superconductivity, and because the existence (or nonexistence) of such a state is an interesting and unanswered question of principle in the theory of quantum antiferromagnetism.

The two-dimensional square lattice spin- $\frac{1}{2}$ QAFM, a reasonable model of spin dynamics in the parent insulators of the superconducting cuprates,³ is now believed to have a Néel-ordered ground state. A variety of theoretical techniques including small cluster diagonalization,^{4,5} variational Monte Carlo,^{6,7} and series expansions of anisotropic Heisenberg models⁸ are all consistent with an ordered ground state retaining 61% of the classical Néel order, in excellent agreement with linear spin-wave theory.⁹

The two-dimensional triangular lattice spin- $\frac{1}{2}$ QAFM was proposed by Anderson¹⁰ to have a spin-liquid ground state. Subsequent theoretical studies have supported the conclusion that the ground state has either very weak or no three-sublattice Néel order,¹¹⁻¹⁵ although linear spin-wave theory predicts¹⁶ Néel order with 48% of the classical staggered magnetization and a variational approach which works well on the square lattice predicts⁷ 68% of the classical Néel order. At $T=0$ this system may be at or near a critical point,^{11,12} making accurate characterization of the ground-state properties difficult using any method short of exact solution.

An argument has been made that the triangular lattice spin- $\frac{1}{2}$ QAFM should have a spin-liquid ground state.¹⁷ The argument given by the authors of Ref. 17 is based on a mapping of the triangular spin- $\frac{1}{2}$ QAFM onto the quantum Hall effect Hamiltonian for electrons in a magnetic field, and con-

cludes that the Kalmeyer-Laughlin $m=2$ wave function,¹⁸ or equivalently a resonating-valence-bond (RVB) state, closely approximates the exact ground state. Our present results do not support this suggestion.

Another candidate for a two-dimensional spin-liquid is the *kagomé* lattice¹⁹ spin- $\frac{1}{2}$ QAFM, which has been studied by small cluster diagonalization,¹⁴ linear spin-wave theory,²⁰ and series expansions about the Ising limit.^{21,12} No convincing evidence of Néel order at $T=0$ has yet been found.

This paper is organized as follows. Section I presents our method of constructing spin- $\frac{1}{2}$ QAFM variational states. On the square lattice, the resulting variational state has been employed previously²² using small clusters. Our approach allows us to confirm these results and extend them to larger embedded clusters, permitting extrapolation to the thermodynamic limit. In Sec. II we consider a pair of bipartite lattices which are believed to exhibit ordered ground states (the square and honeycomb^{26,27} lattices), and show that our variational states yield results in agreement with other calculations. In Sec. III we present results obtained with our variational states on two tripartite lattices whose ground states are controversial (the triangular and *kagomé*). These suggest that the triangular lattice spin- $\frac{1}{2}$ QAFM does possess Néel order, but that the *kagomé* lattice spin- $\frac{1}{2}$ QAFM does not. In Sec. IV we summarize our findings and discuss possible flaws in our approach.

I. VARIATIONAL STATES

We consider variational states for a spin- $\frac{1}{2}$ Heisenberg antiferromagnet, whose Hamiltonian has the form

$$\mathcal{H} = + \sum_{\langle ij \rangle} \mathbf{S}_i \cdot \mathbf{S}_j, \quad (1)$$

where \mathbf{S}_i is the spin operator on site i and the sum runs over all pairs of nearest-neighbor sites i and j .

To obtain our variational states, we start with half-filled Slater determinant states $|\phi\rangle$ with antiferromagnetic order

adjustable between zero and the classical value $m^\dagger = 1/2$. Local number fluctuations in $|\phi\rangle$ are removed by projecting out all configurations having doubly occupied sites (Gutzwiller projection), leaving the variational state

$$|\Psi\rangle \equiv \prod_i (1 - n_{i\uparrow} n_{i\downarrow}) |\phi\rangle. \quad (2)$$

On the square lattice, $|\Psi\rangle$ yields excellent variational energies^{22,23} when the proper correlations are built into the Slater determinant $|\phi\rangle$. This can be achieved by taking $|\phi\rangle$ to be the ground state of a tight-binding Hamiltonian which incorporates a (possibly nonuniform) fictitious magnetic flux coupled to the particles orbital motion, and a staggered magnetic field coupled to spin.²²

Explicitly, $|\phi\rangle$ is the half-filled ground state of the tight-binding Hamiltonian

$$H_\phi = - \sum_{\langle ij \rangle \alpha} e^{ia_{ij}} c_{i\alpha}^\dagger c_{j\alpha} + h \sum_i \hat{\epsilon}_{\mu(i)} \cdot \mathbf{S}_i. \quad (3)$$

Here $c_{i\alpha}^\dagger$ creates a fermion with spin projection α at the site i , and $\mathbf{S}_i = \frac{1}{2} \sum_{\alpha\beta} c_{i\alpha}^\dagger \vec{\sigma}_{\alpha\beta} c_{i\beta}$ is the spin operator at site i . The vector potential a_{ij} describes the fictitious flux, $\mu(i)$ labels the magnetic sublattice to which site i belongs, and $\hat{\epsilon}_\mu$ is a unit vector pointing in the direction of a spin on sublattice μ in a classical Néel ground state. The variational parameter h adjusts the strength of the antiferromagnetic order present in $|\phi\rangle$, and hence $|\Psi\rangle$. It is chosen to minimize the variational energy for a system of N spins,

$$E(h) = \frac{\langle \Psi(h) | \mathcal{H} | \Psi(h) \rangle}{\langle \Psi(h) | \Psi(h) \rangle} = \frac{1}{z} zN \langle \mathbf{S}_i \cdot \mathbf{S}_j \rangle_h, \quad (4)$$

where z is the coordination number of the lattice and sites i and j are nearest neighbors.

The dimensionless ‘‘flux’’ through a plaquette is the directed sum of the phase factors $\sum a_{ij}$ around the plaquette. (In these units a full flux quantum corresponds to a flux of 2π .) The distribution of the a_{ij} ’s is only determined to within a gauge transformation. We choose the flux through each elementary plaquette to be that which minimizes the sum of single-particle energies below the Fermi level on an isolated plaquette.²⁴ Specifically, for n an integer, plaquettes with $4n+2$ sites require no added flux, while those with $4n$ sites require π added flux. Plaquettes with odd numbers of sites require $\pm\pi/2$ added flux. These rules are successful predictors of the best variational state $|\Psi\rangle$ for an infinite periodic lattice, and seem to work on many (though not all) finite systems.²⁵

The proper addition of flux (nonzero a_{ij}) and/or magnetization (nonzero h) in Eq. (3) opens a gap in the spectrum of H_ϕ at the Fermi level, making all physical correlations in $|\phi\rangle$ short ranged. The correlation length ξ is defined by the asymptotic decay of the Green’s function for large separation, $\langle \phi | c_{i\alpha}^\dagger c_{j\alpha} | \phi \rangle \sim e^{-r_{ij}/\xi}$.

On the square and honeycomb lattices, there are two sublattices $\mu \in \{A, B\}$ and we take $\hat{\epsilon}_A = \hat{z}$ and $\hat{\epsilon}_B = -\hat{z}$. On the triangular and *kagomé* lattices, the classical ground state has three sublattices $\mu \in \{A, B, C\}$ whose magnetization directions are 120° apart, e.g., $\hat{\epsilon}_A = \hat{y}$, $\hat{\epsilon}_B = (\sqrt{3}\hat{x} - \hat{y})/2$, and $\hat{\epsilon}_C = -(\sqrt{3}\hat{x} + \hat{y})/2$. On the *kagomé* lattice the three sublattices

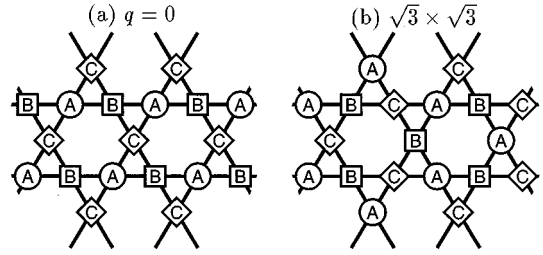


FIG. 1. Possible arrangements of the three magnetic sublattices A , B , and C on the *kagomé* lattice. (a) $q=0$ and (b) $\sqrt{3} \times \sqrt{3}$.

may be arranged in the $q=0$ (3 spins per unit cell) arrangement shown in Fig. 1(a), or the $\sqrt{3} \times \sqrt{3}$ (9 spins per unit cell) arrangement shown in Fig. 1(b). (The latter pattern is obtained by starting with the triangular lattice $\sqrt{3} \times \sqrt{3}$ Néel state and deleting sites to obtain the *kagomé* lattice.)

To compute spin correlations $\langle \mathbf{S}_i \cdot \mathbf{S}_j \rangle$ and sublattice magnetization $m^\dagger(h) \equiv (1/N) \sum_i \langle \hat{\epsilon}_{\mu(i)} \cdot \mathbf{S}_i \rangle_h$, we use the embedded cluster method.²³ Briefly, we consider a small cluster of N_c sites embedded in an infinite system. Correlations within the cluster are computed exactly, while correlations outside the cluster are accounted for only approximately. The thermodynamic limit is usually reached rapidly when the cluster size exceeds the correlation length ξ . This method converges much more rapidly than exact Gutzwiller projection on a series of progressively larger finite systems.²³

II. BIPARTITE LATTICES

On the square lattice, the loop rules described above suggest that each elementary plaquette should have $\Phi_0/2$ flux, i.e., $\sum a_{ij} = \pi$ around each square. For the honeycomb lattice, the rules suggest that no fictitious flux is required through each hexagonal plaquette, and $a_{ij} = 0$. These patterns do *not* break time-reversal or parity symmetry.

For both the square lattice flux state and the fluxless honeycomb state, the $h=0$ spectra of H_ϕ are gapless, although they have vanishing density of states at the Fermi level, and possess particle-hole symmetry. The resulting correlations decay fast enough for the embedded cluster method to converge.²³ When $h \neq 0$, a complete gap is opened in the spectrum for both lattices, and particle-hole symmetry is preserved [see Figs. 2(a) and 2(b)].

Figure 3(a) shows our results computed using embedded clusters containing 8, 12, and 18 sites on the square lattice. These clusters have not yet converged to the thermodynamic limit. For clusters larger than ~ 20 sites we must use a Monte Carlo algorithm²³ to sum over spin configurations, which leads to error bars that blur the variational minimum with respect to m^\dagger . For the 18-site cluster, the extrapolated minimum occurs when $m^\dagger \approx 0.38$, which is within the range of results obtained with other methods.³

Fixing h near the 18-site minimum and extrapolating using clusters containing 8–44 sites as shown in the inset of Fig. 3(a), we obtain a variational energy of $E/N = -0.68 \pm 0.01$, comparable to estimates derived from exact diagonalization of small clusters⁴ and series expansions,⁸ $E/N = -0.677 \pm 0.008$.

For the honeycomb lattice [Fig. 3(b)], we obtain a varia-

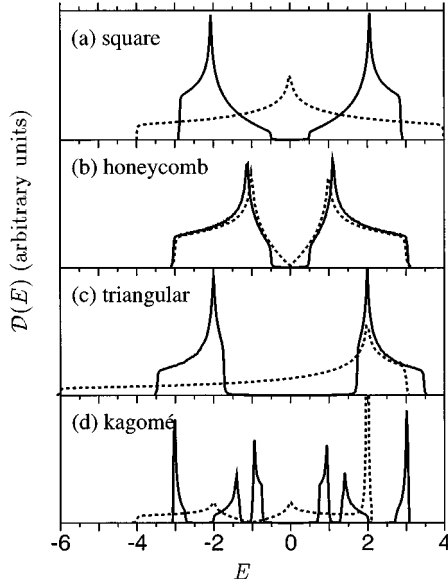


FIG. 2. Density of H_ϕ single-particle eigenstates $\mathcal{D}(E)$ for the lattices studied in this paper. Dashed lines show $\mathcal{D}(E)$ when there is no fictitious flux ($a_{ij}=0$) and no induced Néel order ($h=0$). Solid lines show $\mathcal{D}(E)$ and a fictitious flux as specified by the loop rules in the text, with $h \neq 0$ (a)–(c), $h=0$ (d). Note that the flux and/or induced Néel order opens a gap at half filling, and establishes particle-hole symmetry.

tional minimum near $m^\dagger \approx 0.35$ for all clusters containing more than 10 sites. The extrapolation to larger N is not as smooth as that of the square lattice, so we instead quote the energy associated with the largest cluster we considered ($N=54$ sites), $E/N = -0.54 \pm 0.01$. This compares favorably with estimates of the ground-state energy and staggered magnetization of $E/N = -0.545$ and $m^\dagger = 0.22$ from Monte Carlo,²⁶ $E/N = -0.549$ and $m^\dagger = 0.24$ from second-order spin waves,²⁷ and $E/N = -0.544$ and $m^\dagger = 0.27$ from series expansion.²⁷

A more stringent test of the variational state is obtained by examining the spin-spin correlations at distances farther than nearest neighbor. Table I presents a comparison of the spin-spin correlations computed using large embedded clusters with those obtained by exactly diagonalizing the Heisenberg model on a 32-site square lattice with periodic boundary conditions. As Table I indicates, there is generally good agreement between the spin-spin correlations calculated in our variational state and those calculated by exact diagonalization of small periodic systems. (We do not show comparison with the honeycomb lattice because we are unaware of any exact diagonalizations which report correlation functions.)

III. TRIPARTITE LATTICES

For the triangular lattice, the loop rules prescribe a uniform flux $\Phi_0/4$. For the *kagomé* lattice, the loop rules suggest a uniform flux of $\Phi_0/4$ through the triangles ($\sum a_{ij} = \pi/2$), and 0 through the hexagons. Both of these flux patterns break time-reversal and parity symmetry, but introduce particle-hole symmetry²⁴ into the tight-binding Hamiltonian H_ϕ . Figures 2(c) and 2(d) shows the density of states

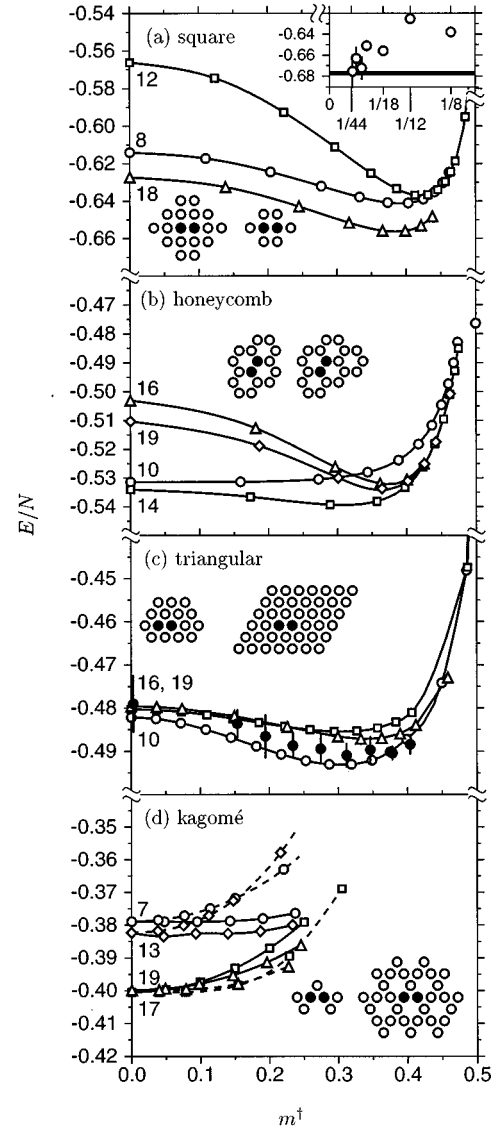


FIG. 3. Variational energy $E(h)$ vs. $m^\dagger(h)$, computed using embedded clusters on (a) square, (b) honeycomb, (c) triangular, and (d) *kagomé* lattices. The lines are guides to the eye; in (d) the solid lines connect results with $q=0$ magnetization, while dashed lines connect those with $\sqrt{3} \times \sqrt{3}$ magnetization (see text). The points in the inset of (a) illustrate the extrapolation of the lowest energy state vs. the inverse of the embedded cluster size $1/N_c$. Also appearing in (a)–(d) are illustrations of some of the clusters used; the spin-spin correlation was computed between sites marked by filled circles.

resulting from these flux patterns.

Figure 3(c) shows $E(h)$ versus $m^\dagger(h)$ for the triangular lattice using embedded clusters. The variational minimum occurs at $m^\dagger \approx 0.3$, indicating a tripartite Néel state rather than a spin-liquid ground state. Using clusters containing as many as 54 sites, we estimate the infinite cluster size variational energy to be $E/N = -0.490 \pm 0.005$. This is substantially higher than the exact energy of a 36-site periodic cluster,¹³ $E/N = -0.56037$.

To investigate possible reasons for this discrepancy, we performed our calculation with $h=0$ on a finite system, rather than an infinite one. Table II shows our results using

TABLE I. Spin-spin correlation function for square, *kagomé*, and triangular spin- $\frac{1}{2}$ QAFM's. The middle column reports our embedded cluster results, while the last column reports the correlations of the largest published exact diagonalizations.

Square lattice $\langle \mathbf{S}_i \cdot \mathbf{S}_j \rangle$		
r_{ij}	44 site cluster	Ref. 5 (32 sites)
1	-0.335 ± 0.013	-0.3401
$\sqrt{2}$	$+0.204 \pm 0.002$	$+0.2090$
2	$+0.188 \pm 0.002$	$+0.1874$
$\sqrt{5}$	-0.179 ± 0.002	-0.1830
Triangular lattice $\langle \mathbf{S}_i \cdot \mathbf{S}_j \rangle$		
r_{ij}	42 site cluster	Ref. 13 (36 sites)
1	-0.163 ± 0.002	-0.1868
$\sqrt{3}$	$+0.161 \pm 0.002$	$+0.1535$
2	-0.065 ± 0.002	-0.0548
$\sqrt{7}$	$+0.076 \pm 0.002$	-0.0066
Kagomé lattice $\langle \mathbf{S}_i \cdot \mathbf{S}_j \rangle$		
r_{ij}	52 site cluster	Ref. 14 (36 sites)
1	-0.205 ± 0.004	-0.2192
$\sqrt{3}$	-0.007 ± 0.004	$+0.0116$
2 (in line)	$+0.032 \pm 0.004$	$+0.0527$
2 (across hexagon)	-0.028 ± 0.004	-0.0090

lattices of sites which have L and M sites in each of the two lattice translations of the triangular lattice and whose boundary conditions are periodic.

We find that our variational state does indeed have a lower energy on these small triangular lattice systems than in our embedded cluster calculation for an infinite system. In fact, all of the $L=2$ systems we studied have an energy below that reported in the literature for the energy extrapolated to infinite system size. [We note that because our variational state is constructed from Hamiltonians of the type Eq. (3), some of the small periodic systems studied in the literature are essentially inaccessible because they do not decompose into magnetic unit cells when the flux state is constructed. That is, adding flux to these systems requires a net fictitious flux through the system which is not a multiple of the flux quantum 2π .] On the other hand, the single $L=4$ system accessible to us has an energy above even our em-

TABLE II. Energy per site E/N for the variational state Eq. (2) with $h=0$ on small triangular lattices with periodic boundary conditions. The lattice dimensions are L and M in each of the two fundamental lattice translations of the triangular lattice, and contain $N=LM$ sites.

System size ($L \times M$)	E/N
2×2	-0.500 000
2×4	-0.701 283
2×6	-0.686 685
2×8	-0.629 483
4×4	-0.459 370

bedded cluster results. This strong boundary condition dependence suggests that the discrepancy between the energy we report for the triangular lattice and those reported for exact diagonalization of small periodic lattices is due to the difference in lattice boundary conditions, which affects the energy on the triangular lattice more strongly than on the other lattices. This is somewhat surprising, since for these states the spin-spin correlations decay exponentially, and one might therefore expect less dependence on boundary conditions.

Figure 3(d) shows $E(h)$ versus $m^\dagger(h)$ for the *kagomé* lattice using embedded clusters, for both the $q=0$ and $\sqrt{3} \times \sqrt{3}$ magnetization patterns. In both cases the variational minimum occurs at $h=0$, indicating a disordered ground state. Our estimate of the variational energy, considering clusters containing as many as 52 sites, is $E/N = -0.409 \pm 0.006$. As with the triangular lattice, this number is significantly higher than that yielded by exact diagonalization of a finite 36-site cluster,¹⁴ $E/N = -0.438 38$.

To confirm that our variational states have the same character as the true ground states, we can again compare further range spin-spin correlations with exact diagonalization studies of 36-site periodic clusters of the triangular¹³ and *kagomé*¹⁴ lattices (Table I). Qualitatively, the agreement with exact diagonalization results is similar to that obtained on bipartite lattices. In contrast with the bipartite lattices, correlations on the tripartite lattices decay very rapidly, to near zero on the *kagomé* lattice and to a weak three-sublattice order on the triangular lattice. These longer-range correlations, however, are consistently larger in our calculations than in the exact diagonalization studies.

IV. CONCLUSIONS

The variational state $|\Psi\rangle$ appears to be a good approximation to the true ground state as measured by its variational energy and, more significantly, because the short-range correlations match those of the ground state. In agreement with other calculations on the square and honeycomb lattice spin- $\frac{1}{2}$ QAFM, our best variational states exhibit Néel order. On the triangular lattice, our best variational state also contains Néel order, with $m^\dagger \approx 0.3$. In sharp contrast, our best variational state for the *kagomé* lattice spin- $\frac{1}{2}$ QAFM contains no staggered magnetization for any simple unit cell. This strongly suggests that the *kagomé* lattice spin- $\frac{1}{2}$ QAFM has a disordered ground state.

As with any variational calculation, errors in the “ground state” order may result from an insufficiently general class of trial states. The variational states we consider overestimate the importance of Néel order in obtaining an energy minimum; our predicted staggered magnetizations are roughly 20% larger than obtained by other methods. These overestimates of Néel order on the square and honeycomb lattice suggest that the states we consider are overly prone to developing antiferromagnetic order. This may explain why this class of variational state predicts Néel order on the triangular lattice while other methods do not.

Our previous work²³ leads us to believe that the finite-size effects associated with clusters embedded into an infinite system are generally of the same magnitude as those associated with a finite system. Thus the actual energy of the infi-

nite triangular and *kagomé* Heisenberg spin lattices is probably somewhere between our estimates presented here and those published estimates arising from exact diagonalization of finite systems.

Our variational states currently do not allow for the possibility of spin-Peierls ordering. This could easily be remedied by allowing the hopping matrix elements in Eq. (3) to vary in magnitude from bond to bond.

ACKNOWLEDGMENTS

Ames Laboratory is operated for the U.S. Dept. of Energy by Iowa State University under Contract No. W-7405-Eng-82. This work was supported in part by the director for Energy Research, Office of Basic Energy Sciences. Work at Berkeley was supported by the NSF under Grant No. DMR-91-57414 and by the U.S. Dept. of Education. D.S.R. acknowledges a grant from the Alfred P. Sloan Foundation.

-
- ¹F.D.M. Haldane, Phys. Rev. Lett. **50**, 1153 (1983).
²P.W. Anderson, Science **235**, 1196 (1987); in *Frontiers and Borderlines of Many-Particle Physics*, edited by J.R. Schrieffer (North-Holland, Amsterdam, 1987).
³E. Manousakis, Rev. Mod. Phys. **63**, 1 (1991), and references therein.
⁴S. Tang and J.E. Hirsch, Phys. Rev. B **39**, 4548 (1989); S. Tang and H.Q. Lin, *ibid.* **38**, 6863 (1988).
⁵H. Q. Lin, Phys. Rev. B **42**, 6561 (1990).
⁶H. Yokoyama and H. Shiba, J. Phys. Soc. Jpn. **56**, 3570 (1987).
⁷D.A. Huse and V. Elser, Phys. Rev. Lett. **60**, 2531 (1988).
⁸D. Huse, Phys. Rev. B **37**, 2380 (1988); R.R.P. Singh, *ibid.* **39**, 9760 (1989).
⁹R. Kubo, Phys. Rev. **87**, 568 (1952).
¹⁰P.W. Anderson, Mater. Res. Bull. **8**, 153 (1973).
¹¹S. Fujiki and D.D. Betts, Can. J. Phys. **65**, 489 (1986); Prog. Theor. Phys. Suppl. **87**, 268 (1986).
¹²R.R.P. Singh and D. Huse, Phys. Rev. Lett. **68**, 1766 (1992).
¹³P.W. Leung and K.J. Runge, Phys. Rev. B **47**, 5861 (1993).
¹⁴P.W. Leung and V. Elser, Phys. Rev. B **47**, 5459 (1993).
¹⁵Y.-C. Chen, A. Moreo, F. Ortolani, E. Dagotto, and T. K. Lee, Phys. Rev. B **50**, 655 (1994).
¹⁶S.J. Miyake, Prog. Theor. Phys. **74**, 468 (1985).
¹⁷K. Yang, L.K. Warman, and S.M. Girvin, Phys. Rev. Lett. **70**, 2641 (1993).
¹⁸V. Kalmeyer and R.B. Laughlin, Phys. Rev. Lett. **59**, 2095 (1987).
¹⁹The Japanese word *kagomé* refers to a type of bamboo weave. The *kagomé* lattice is the lattice formed by placing one site at the center of each intersection of bamboo reeds in *kagomé*. See I. Syôzi, Prog. Theor. Phys. **6**, 306 (1951).
²⁰A.B. Harris, C. Kallin, and A.J. Berlinsky, Phys. Rev. B **45**, 2899 (1992).
²¹M.P. Gelfand, R.R.P. Singh, and D.A. Huse, Phys. Rev. B **40**, 10 801 (1989); M.P. Gelfand, *ibid.* **42**, 8206 (1990).
²²T.C. Hsu, Phys. Rev. B **41**, 11 379 (1990).
²³A. Barbieri, D.M. Deaven, and D.S. Rokhsar, Phys. Rev. B **45**, 8288 (1992); D.M. Deaven, D.S. Rokhsar, and A. Barbieri (unpublished).
²⁴D.S. Rokhsar, Phys. Rev. Lett. **65**, 1506 (1990).
²⁵D.M. Deaven (unpublished).
²⁶J.D. Reger, J.A. Riera, and A.P. Young, J. Phys. C **1**, 1855 (1989).
²⁷J. Oitmaa, C.J. Hamer, and Z. Weihong, Phys. Rev. B **45**, 9834 (1992).